

Study of the Dislocation and Luminescence Intensity Distributions of Gallium Nitride LED on the Carbon-Nanotubes Patterned Sapphire Substrate

Mingsheng Xu¹, Yang Wei^{2,*}, Shuang Qu³, Chengxin Wang³, Xiaobo Hu¹ and Xiangang Xu^{1,3,*}

¹Institute of Crystal Materials, Shandong University, Jinan, 250100, China.

²Department of Physics and Tsinghua-Foxconn Nanotechnology Research Center, Tsinghua University, Beijing, 10000, P. R. China.

³Shandong Inspur Huaguang Optoelectronics Co., Ltd., Jinan, 250101, China

*E-mail: weiyang@mail.tsinghua.edu.cn; xxu@sdu.edu.cn.

Received: 23 February 2014 / *Accepted:* 12 March 2014 / *Published:* 14 April 2014

Gallium nitride (GaN) films have been grown on the sapphire substrate with and without carbon-nanotubes (CNTs). The stripy defects distribution of the GaN film on the CNTs patterned sapphire substrate (CPSS) coincides with the morphology of the CNTs bundles. The localized dislocation density of the GaN layer near the CNTs on the CPSS decreases to $4.72 \times 10^7 \text{ cm}^{-2}$. The confocal scanning electroluminescence microscopy image of the GaN LED on CPSS reveals stripy luminescence intensity distribution. The results directly demonstrate that the CNTs can reduce the dislocation of the GaN film and improve the electrical and optical properties of the GaN LED.

Keywords: carbon nanotubes, gallium nitride, dislocation density,

1. INTRODUCTION

Gallium nitride (GaN) is an ideal semiconductor material in the fields of optoelectronics and microelectronics because of its excellent physical properties. Foreign substrates such as sapphire[1], silicon carbide[2] and silicon[3] are often used for GaN epitaxial growth because of the lack of affordable large area GaN substrates. Due to its low price and high transmittance, sapphire is the most common substrate used for GaN growth. However, the defects propagate from the interface of GaN/sapphire into the surface, deteriorating electrical and optical properties of GaN-based devices. Therefore, the way to reduce the dislocations density needs to be developed to enhance the reliability of nitride devices.

It has been proved that the density of the dislocations in GaN hetero-epitaxial layers can be

effectively reduced by various techniques [4-6]. The epitaxial lateral overgrowth (ELOG) technology developed by Kato et al. is an efficient method to eliminate the density of dislocation with a patterned dielectric mask [7]. The electrochemical behaviors of carbon nanotubes (CNTs) have been reported by Yang etc [8]. Recently, CNTs were proposed to improve the GaN quality by ELOG[9]. However, the mechanisms of dislocation reduction and optical power improvement of GaN LED grown on carbon nanotube-patterned sapphire substrate (CPSS) still need to be further studied.

Here we have grown GaN films and fabricated InGaN/GaN LEDs by metal-organic chemical vapor deposition (MOCVD) on CPSS and the conventional sapphire substrate (CSS). The stripy distribution of the dislocations from the cathode luminescence (CL) image of the GaN film on CPSS demonstrates that CNTs can improve the crystallization quality of the GaN layer by the epitaxial lateral overgrowth process. Besides, the strip pattern of the luminous intensity from the confocal scanning electroluminescence microscopy (CSEM) image of the GaN LED on CPSS coincides with the stripy distribution of the dislocations. The results directly reveal that the lower dislocation density can enhance the light intensity of the GaN LED.

2. EXPERIMENTS

Super-aligned multi-walled carbon nanotube (MWCNT) arrays were grown on silicon wafers by a low-pressure chemical vapor deposition (LPCVD)[10, 11]. The diameter of the CNTs in the super-aligned arrays is about 15nm. Aligned CNT films were continuously dry spun from the CNT array and then coated on 2-inch c-plane sapphire wafers with CNT alignment perpendicular to the (11-20) using a focused laser beam[9].

C-plane CPSS and CSS were used as the substrates for GaN films growth by metal-organic chemical vapor deposition (MOCVD). The SEM images of the CPSS and CSS are shown in figure 1. The CNTs arrays show a stripy pattern on sapphire substrate, as shown in figure 1 (a). Hydrogen and nitrogen were used as carrier gas while trimethyl gallium (TMG), trimethyl indium (TMI), trimethyl aluminium (TMAI), and ammonia (NH₃) were used as sources of Ga, In, Al, and N, respectively. The growth of GaN template was performed following the three steps: (1), we deposited about 30 nm nucleation layer at 530 °C; (2), the temperature was increased to 1050°C while the pressure of the reactor kept 658 mbar. About 2 μm rough GaN layer was grown on the top of the buffer layer; (3), the temperature and the pressure of the reactor were changed to 1090 °C and 263 mbar, respectively. The recovery layer with a thickness of 3μm was deposited on the rough layer. After that, a 2-μm Si-doped n-type GaN with a doping concentration of $1 \times 10^{19} \text{cm}^{-3}$ was grown on the GaN template. In addition, twelve pairs of InGaN/GaN multi-quantum wells (MQWs) with 3-nm-thick quantum well and 10-nm-thick quantum barrier were grown on the top of the n-type GaN layer. The growth temperature of the wells and barriers were 750 °C and 850 °C, respectively. The epitaxial structures were finally covered with a 300-nm-thick p-GaN layer. The Mg dopant concentration of the p-GaN is $5 \times 10^{19} \text{cm}^{-3}$. For comparison, the GaN films were also grown on the CSS at the same conditions.

After the epitaxial growth, the wafers were defined with mesa size of 200 μm × 500 μm by a standard photolithographic process and partially dry-etched down to the n-type GaN by inductively

coupled plasma (ICP) technology. A transparent conduction indium-tin-oxide (ITO) thin film and Cr-Ti-Au metals were deposited as the p-type ohmic contact layer and electrodes with an evaporation method.

Field emission scanning electron microscopy (FE-SEM) and atomic force microscopy (AFM) were used to observe the surface morphologies of the GaN films grown on CPSS and CSS at different growth stages. The CL measurements were used to evaluate the crystal quality of n-type GaN film. A confocal scanning electroluminescence microscopy (CSEM) was employed to investigate the microscopic electroluminescence (EL) properties of the GaN LEDs fabricated on CPSS and CSS.

3. RESULTS AND DISCUSSIONS

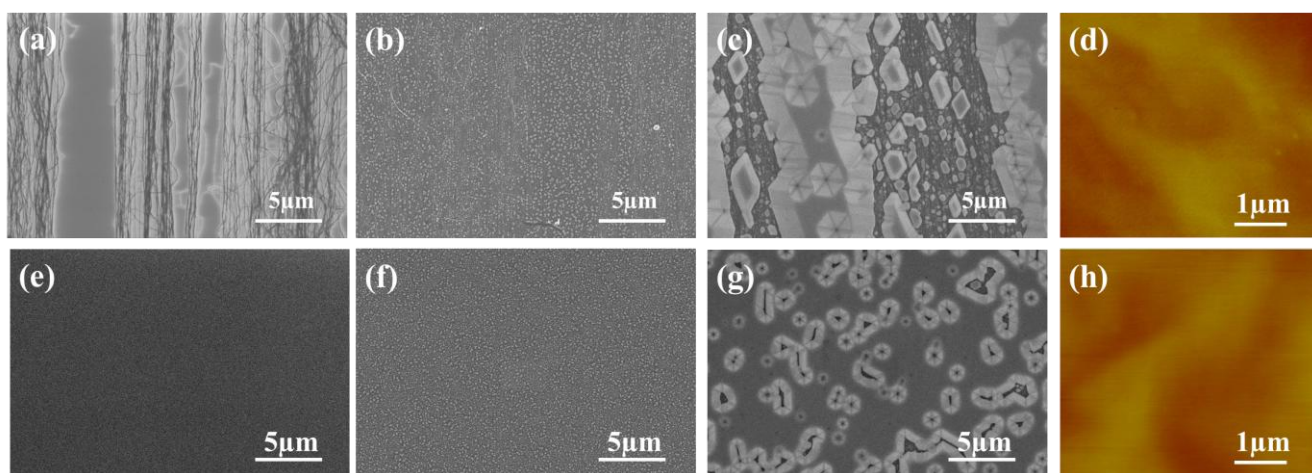


Figure 1. The surface morphologies of the substrates and the GaN films: (a) and (e) SEM images of CPSS and CSS; (b) and (f) SEM images of GaN nucleation layers on CPSS and CSS; (c) and (g) SEM images of GaN rough layers on CPSS and CSS; (d) and (h) AFM images of the recovery layers on CPSS and CSS;

Figure 1 (b) and (f) show the morphologies of the GaN nucleation layers on CPSS and CSS. The nucleation islands distributions of the two samples have much difference. As shown in the figure 1 (f), the GaN islands distribute uniformly on CSS. However, the GaN nucleation islands distribute in a stripy pattern on CPSS, as shown in the figure 1 (b). The islands crowd together in the area without CNTs. There are hardly any islands distributed near the CNTs arrays. The nucleation islands distribution on CPSS coincides with the morphology of CNTs. The results show that the CNTs on CPSS affect the distribution of the GaN nucleation islands because of the absence of adhesion of reactant gas [9]. The nucleation islands grow up to big hills in the next epitaxial coalescence process. If the nucleation islands is enough dense, the hills will connect together and form a flat surface with small hexagonal pits, as shown in the figure 1 (g). The similar morphology can be seen from the region without CNTs of the GaN film on CPSS. The islands are too sparse to form a flat surface near the CNTs during the rough growth process. As a result, the stripy pattern rough GaN layer on CPSS can be seen from figure 1 (c). The SEM images of the GaN layers on CPSS and CSS demonstrate that the

CNTs can influence the morphologies of the GaN films. The stripy distribution CNTs act as a native mask during the GaN films growth process. After the growth of recovery layer, the GaN layers grown on CPSS and CSS become smooth surfaces. The surface morphologies of the recovery GaN layers on CPSS and CSS were characterized by AFM measurements, as shown in figure 1(d) and (h). The root mean square (RMS) roughness of GaN films grown on CPSS is similar to that grown on CSS, as shown in the table I. The results demonstrate that the superior flat surface of the GaN films grown on the CPSS and CSS meet the requirements of MQWs growth for LED applications.

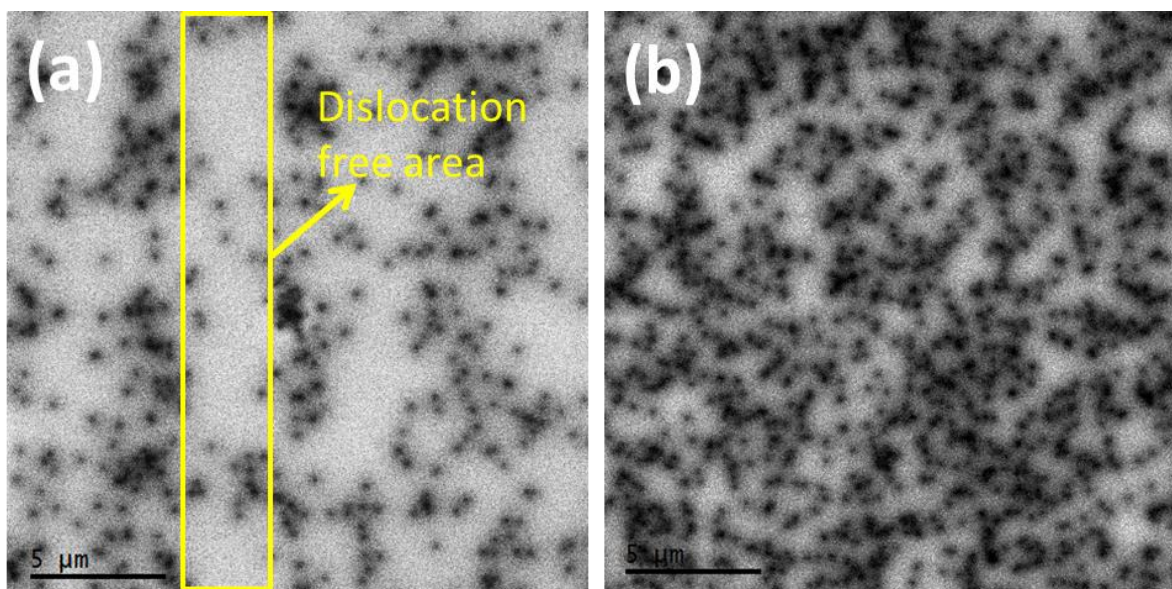


Figure 2. CL images of GaN recovery layers grown on: (a) CPSS; (b) CSS.

Figure 2 shows the CL images of the recovery GaN layers on CPSS and CSS. The dislocations of the GaN films are associated with the dark spots in the CL images because of their non-radiative recombination character [12]. The density of dark spots shown in the CL images is close to the dislocation density of GaN films. Table I shows the dislocation densities of the two samples calculated from the number of dark spots of CL images. The average dislocation density of GaN film grown on CPSS decreases by 63% compared with that of GaN film on CSS. Besides, the homogeneous distribution of the dark spots can be seen in the CL image of GaN on CSS while stripy distribution can be seen on CPSS, as shown in figure 2 (b). The stripy pattern of the CL image shown in figure 2 (a) is consistent with that of SEM image shown in figure 1 (c). The stripy pattern of the dislocations originates from the CNTs bundles distribution of the CPSS. The CNTs bundles in the figure 1 (a) act as native mask for the GaN growth. The GaN nucleation islands cannot grow on the CNTs because of the poor soak property. The big islands away from the CNTs grow up to hills during the rough layer process. In the next stage, the GaN growth mode changes to two-dimension (2D) from 3D because of the higher growth temperature and the lower growth pressure. The gaps between the hills shown in figure 1 (b) are filled by the lateral growth of the GaN layers in the 2D growth mode. The dislocations can bend in the coalescence process at the spaces between the hills[13]. As a result, the dislocation

density of the GaN film on the top of the CNTs bundles decreases to about $4.72 \times 10^7 \text{ cm}^{-2}$. The stripy distribution of the dislocations in figure 2 (a) coincides with the stripy pattern of the CNTs bundles shown in figure 1 (a). The results are direct evidence that the CNTs can improve the crystal quality of the GaN film.

Table I. RMS roughness and dislocation density of GaN layers grown on CPSS and CSS.

Sample	RMS roughness(nm)	Dislocation density (cm^{-2})
CPSS	0.75	1.04×10^8
CSS	0.68	2.81×10^8

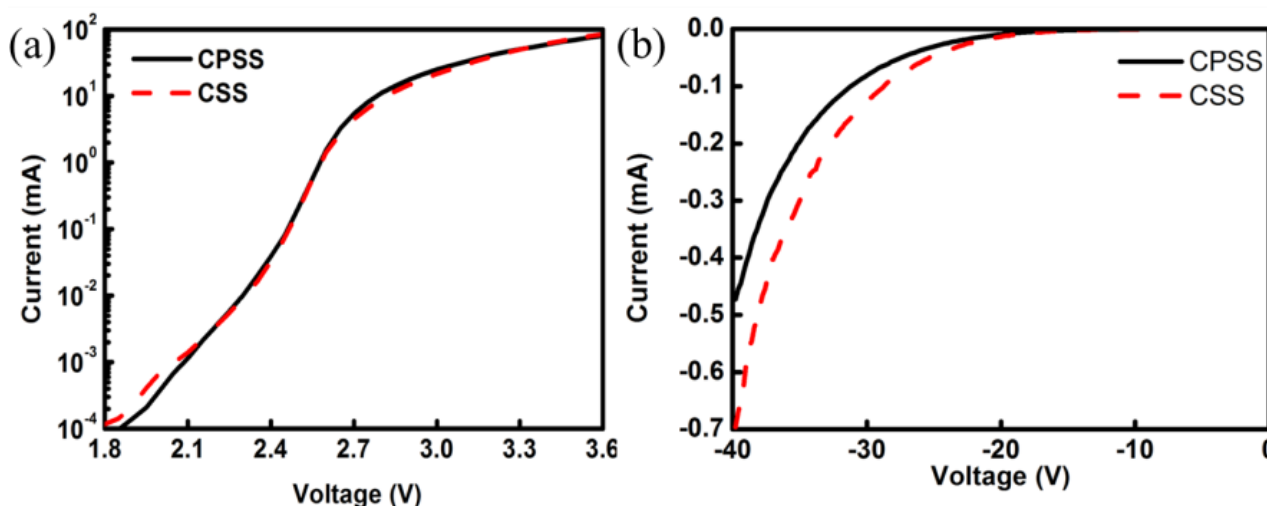


Figure 3. (a) The forward current and (b) reverse current as functions of the voltage of the GaN LED on CPSS and CSS;

We fabricated GaN based LED on CPSS and CSS in order to study the influence of the CNTs bundles on the electrical and optical properties. The current-voltage curves of the GaN LEDs on CPSS and CSS are shown in figure 3. When the forward voltage is smaller than 2.1V, the leakage current of GaN LED on CPSS is lower than that of GaN LED on CSS, as shown in figure 3 (a). The similar phenomenon can be seen in the reverse current-voltage curves of the two samples, as shown in figure 3(b). The reverse leakage current of GaN LED grown on CPSS decreases by 32% at -40 V offset voltage. The leakage current reduction originates from the the reduction of the dislocation density[14]. Thus, the smaller leakage current of GaN LED on CPSS proves indirectly that the CNTs can efficiently reduce the dislocation density of the GaN films.

The CSEM measurements were carried out to further determine the light intensity enhancement of the GaN LED on CPSS. Figure 4 shows the luminescence intensity distributions of the GaN LED on CPSS and CSS. The darker colour means lower light intensity. Figure 4 (b) shows the CSEM image of the GaN LED on CSS. The bright spots and dark spots randomly distribute. However, the light

intensity of the GaN LED on CPSS distributes in bright and dark stripes, as shown in figure 4 (a). The corresponding CL image is shown in figure 2 (a). It is amazing that the EL intensity distribution of the GaN LED on CPSS coincide with the dislocations distribution.

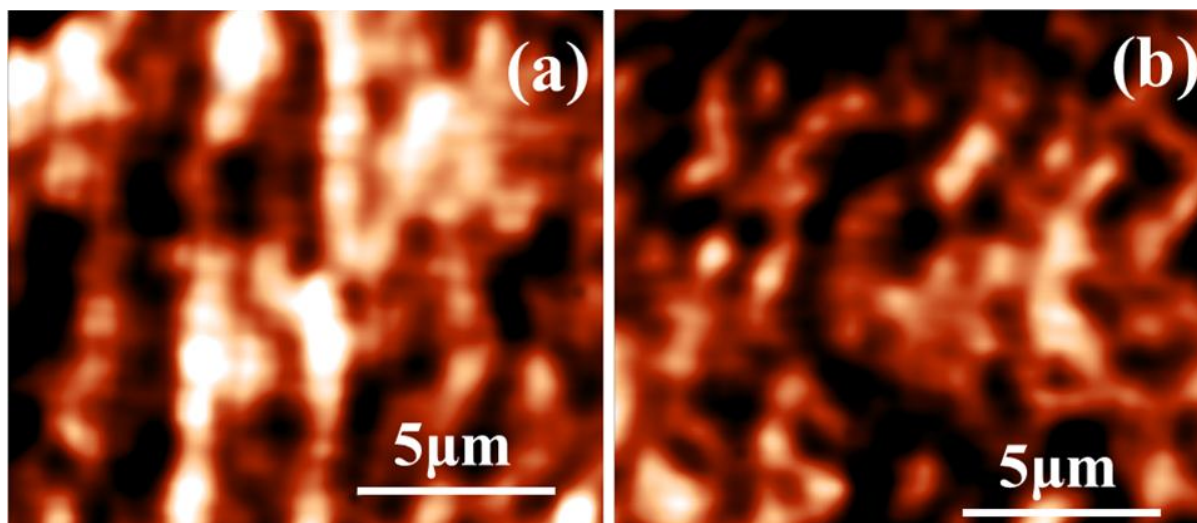


Figure 4. CSEM images of GaN LEDs grown on: (a) CPSS; (b) CSS.

The results directly reveal the influence of the dislocation density on the light intensity of GaN based LED. The experiments demonstrate that the lower dislocation density will lead to the higher luminescence intensity.

4. CONCLUSIONS

We have grown GaN films on CPSS and CSS by MOCVD and fabricated the LED chips with a size of $200 \mu\text{m} \times 500 \mu\text{m}$. Because of the poor soak of the CNTs bundles, the big GaN nucleation islands distribute in stripy pattern, which leads to a stripy morphology of the rough layer GaN on CPSS. The smooth GaN film with low dislocation density was obtained on CPSS because the dislocations bended during the 2D growth process. The stripy distributions of the dislocations from the CL image directly verify the influence of the CNTs on the crystal quality improvement of the GaN film. The localized dislocation density of the GaN layer near the CNTs on the CPSS decreases to $4.72 \times 10^7 \text{ cm}^{-2}$. The low leakage current of the GaN LED on CPSS further confirm dislocation density reduction of the GaN layer. The reverse leakage current decreases by 32% at -40V reverse offset. The strip pattern from the CSEM image of the LED on CPSS coincide with the stripy dislocation distribution from the CL image of the GaN film. The experimental data directly reveal that the lower dislocation density will lead to the higher luminous intensity.

ACKNOWLEDGEMENTS

This work was supported by National Basic Research Program of China under grant No. 2011CB301904, No. 2012CB932301 and No. 2009CB930503, Natural Science Foundation of China

under grant No. 51021062, 11134006 and 51102147. The authors thank Min Han and Shuming Zhang for the helps of the CSEM and CL measurements.

References

1. M. Iwaya, T. Takeuchi, S. Yamaguchi, C. Wetzel, H. Amano, and I. Akasaki, *Japanese Journal of Applied Physics* 37 (1998) 316.
2. R. Wei, X. Chen, L. Wang, S. Song, K. Yang, X. Hu, Y. Peng, and X. Xu, *International Journal of Electrochemical Science* 8(2013), 7099.
3. C. A. Tran, A. Osinski, R. Karlicek, and I. Berishev, *Applied physics letters* 75 (1999) 1494.
4. J.-C. Song, S.-H. Lee, I.-H. Lee, K.-W. Seol, S. Kannappan, and C.-R. Lee, *Journal of Crystal Growth* 308 (2007) 321.
5. Y. Lee, J. Hwang, T. Hsu, M. Hsieh, M. Jou, B. Lee, T. Lu, H. Kuo, and S. Wang, *Photonics Technology Letters, IEEE* 18 (2006) 1152.
6. S. I. S Tanaka, Y Aoyagi, *Applied Physics Letters* 69 (1996) 4096
7. Y. Kato, S. Kitamura, K. Hiramatsu, and N. Sawaki, *Journal of Crystal Growth* 144 (1994) 133.
8. J. Yang, S.-C. Wang, X.-Y. Zhou, and J. Xie, *International Journal of Electrochemical Science* 7(2012), 6118.
9. H. Long, Y. Wei, T. Yu, Z. Wang, C. Jia, Z. Yang, G. Zhang, and S. Fan, *Nano Research* 5 (2012) 646.
10. K. Jiang, Q. Li, and S. Fan, *Nature* 419 (2002) 801.
11. K. Jiang, J. Wang, Q. Li, L. Liu, C. Liu, and S. Fan, *Advanced Materials* 23 (2011) 1154.
12. J. Napierala, D. Martin, N. Grandjean, and M. Ilegems, *Journal of crystal growth* 289 (2006) 445.
13. Y. B. Tao, T. J. Yu, Z. Y. Yang, D. Ling, Y. Wang, Z. Z. Chen, Z. J. Yang, and G. Y. Zhang, *Journal of Crystal Growth* 315 (2011) 183.
14. P. Kozodoy, J. Ibbetson, H. Marchand, P. Fini, S. Keller, J. Speck, S. DenBaars, and U. Mishra, *Applied physics letters* 73 (1998) 975.

© 2014 The Authors. Published by ESG (www.electrochemsci.org). This article is an open access article distributed under the terms and conditions of the Creative Commons Attribution license (<http://creativecommons.org/licenses/by/4.0/>).